ISSN 1560-8034, 1605-6582 (On-line), SPQEO, 2018. V. 21, N 4. P. 336-344.

Semiconductor Physics

Nature and kinetics of paramagnetic defects induced by beta-irradiation of chitosan

A.A. Konchits, B.D. Shanina, I.B. Yanchuk, S.V. Krasnovyd*

V. Lashkaryov Institute of Semiconductor Physics, NAS of Ukraine, 03680 Kyiv, Ukraine
** E-mail: sergkrasnovyd88@gmail.com*

Abstract. A set of chitosan samples irradiated by electrons with various doses were studied using the EPR method. Two kinds of paramagnetic defects PC1 and PC2 initiated by this irradiation due to the breakage of bonds in positions C5 and C1 of the chitosan structure are revealed in the "amorphous" and "crystalline" samples of chitosan. The structure of defects, their spectroscopic parameters, and kinetics of accumulation/decay have been established for the first time. It is found that EPR spectrum of the "crystalline" samples consists of 10 almost equidistant lines of the super-hyperfine (SHF) structure with the splitting between them A = 7.4 G for PC1 center, and a single wide line with the markedly different g-value, attributed to the PC2 one. Both these lines are also present in powder "amorphous" samples, but the SHF structure of the PC1 centers in them is not registered because of broadening the individual SHF components. Kinetics of defect accumulation with increasing dose D of the irradiation, and their gradual disappearance during prolonged storage of samples in air was discovered and studied. Kinetic equations were solved, and the D-dependence and decay times were found from the comparison of theoretical results with the experimental ones. It has been shown that the concentration of shallow and deep traps for electrons affect the rate of the decay process. The recovery process is much slower in the samples having a more perfect crystalline structure.

Keywords: chitin, chitosan, EPR, β-irradiation, super-hyperfine splitting.

doi: https://doi.org/10.15407/spqeo21.04.336
PACS 61.82.Pv, 76.30.Rn, 82.35.Pq, 87.53.Ay, 87.80.Lq

Manuscript received 01.11.18; revised version received 00.00.18; accepted for publication 00.00.18; published online 00.00.18.

1. Introduction

Chitin and its deacetylated derivative chitosan (see Fig. 1) possess unique physical and chemical properties. Chitin and chitosan are non-toxic, bioactive, biocompatible, and widely applicable, in particular, both in the nanoparticle form and antioxidant in anticancer therapy, in theranostics, and so on. They have antimicrobial activity, are able to absorb heavy metals [3, 11, 14-16, 19, 22, 25] and used as a hemostatic (like to Celox) and antimutagenic drugs [23]. In recent years, chitosan has been used in biosensors [12], as well as in composite chitosan-Ag NPs as SERS substrate [18].

Chitin is a linear polysaccharide with unbranched chains composed of elementary units 2-acetamido-2-deoxy-D-glucose, connected by the glycosides bonds. The macromolecule of natural chitin contains a small amount of units with the free primary amino group NH_3. The large length of the chain and its flexibility help to create a complicated super-molecular structure of highly oriented macromolecules of 15…25 nm in length, consisting in turn of micro-fibrils with ~3 nm in diameter for α-chitin [13]. The giant β-chitin crystallites (~50 nm in diameter, ~3 μm in length) were observed for chitin embedded into a protein matrix [5].

Chitosan is usually obtained by the treatment of chitin with the 40…50% aqueous NaOH solution at 110…140 °C [11]. According to the nomenclature of the European Chitin Society (EUCHIS), chitin and chitosan are determined through the degree of insolubility (chitin) or solubility (chitosan) in the acetic acid [8, 20].

The main methods of the chitin or chitosan modification amount to the reduction of the molecular weight, MW, due to destroying the amino group by γ- and β-irradiation, ultrasonic treatment, as well as by mixing with various chemical solvents, additives or doping of the material with hydrogen. In the case of ionizing radiation, it can lead to breaking the chitin/chitosan chains, bond crossing and opening the rings, which results in the irreversible chemical change. The radiolysis degradation mechanism of chitosan was studied at various temperatures by using γ-^{60}Co rays with doses of 5 to 300 kGy [2, 4]. Participation of the amino groups in the mechanism of radiolysis is one of the important problems of chitosan radiation stability because this treatment can produce toxic effects.

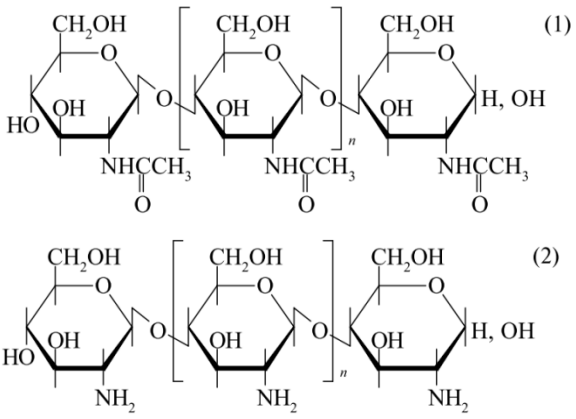

Fig. 1. Chemical structures of chitin (1) and chitosan (2).

The electron microscopy, FTIR, Raman spectroscopy and electron paramagnetic resonance (EPR) are used to study the degradation products and modified structure of the chitosan. The EPR play a specific role, since it is the direct method for studying the properties of any paramagnetic centers (PC) produced under irradiation.

In [6, 24], the EPR spectra have clearly shown a significant effect of chitosan on the suppression of the superoxide anion radicals and lipid radicals of the linoleic acid. Depending on the source and production way of the chitin and chitosan, the presence of PC with the *g*-factor of 2.0012 to 2.0035 is shown. The multicomponent EPR spectra were recorded in [4] for the chitosan after γ- or e-beam irradiation. At doses above 200 kGy, a new signal consisting of asymmetric triplet with an overall splitting of 68 G belonging to nitroxyl-type radicals have been detected.

The present study is devoted to the nature and kinetic characteristics of PC, induced in chitosan by β-irradiation in low sterilization doses 5…35 kGy at room temperature. Based on the highly resolved super-hyperfine structure (SHFS), observed for the first time, the nature of the centers designated as PC1 and PC2 has been established. The dynamic and kinetic characteristics of PC, and the ability of system to recover after β-irradiation have been investigated.

2. Materials and methods

Samples of the commercial chitosan were used after preliminary cleaning. Part of the obtained powdered samples (hereinafter denoted as X1) was undergone to recrystallization in the study process (hereinafter denoted as X2). Paramagnetic properties of the samples were studied both before and after irradiation with a beam of fast electrons with energy of 2 MeV, which was carried out by means of an accelerator ILA-6. EPR measurements were carried out at room temperature using the X-band spectrometer "Radiopan" SE/X-2244. The concentration of PC was determined using the reference sample $MgO:Cr^{3+}$ ($g = 1.9799$) with the number of spins $N_s = 3.4 \cdot 10^{14}$. Paramagnetic properties were also studied briefly in some subsidiary materials that are commonly used in production of Celox (solvents, fillers *etc*.). Samples were put in the silica tubes produced by Wilmad–Lab glass firm, which have no false EPR signals.

3. Results and discussion

3.1. General characteristics of the EPR spectra

Fig. 2 represents EPR spectra of the initial chitosan sample X1, initial and purified celox samples and sample of the solvent (succinic acid) before irradiation. The chitosan and Celox samples show the intensive wide EPR signals with $g \approx 2.55$, $\Delta H_{pp} \sim 0.6$ kG for chitosan, and $g \approx 2.37$, $\Delta H_{pp} \sim 1.3$ kG for Celox sample. These signals are similar to those observed earlier in [9], and can be attributed to uncontrolled impurities of iron oxides. In addition, there is a narrow line in the spectrum of Celox sample with $g \approx 2.004$, $\Delta H_{pp} \sim 10$ G (Fig. 2, curve *2*), where characteristics of which coincide with those for the structure defects revealed in [21]. In the spectrum of X1 samples, there is a narrow line as well (Fig. 2, insert), but its origin is associated with nitroxyl-type radicals [4]. In the recrystallized samples X2, the EPR signals are absent. After purification, all the iron related signals essentially decrease, see for example (Fig. 2, curve *3*). In purified samples X1, a signal from nitroxyl radicals is still recorded.

After irradiation, the paramagnetic properties of the samples X1 and X2 (further only these samples will be studied) change significantly, demonstrating strong EPR signals. Fig. 3a shows, for example, the ESR spectrum of sample X1 after irradiation with the dose of 25 kGy. It is seen that spectrum is a single line with some bend in the center of the spectrum.

In contrast, the EPR spectrum of sample X2 (Fig. 3b) demonstrates well resolved super-hyperfine splitting (SHFS). Preliminary analysis of this spectrum showed that it consists of 5 low-field lines, belonging to

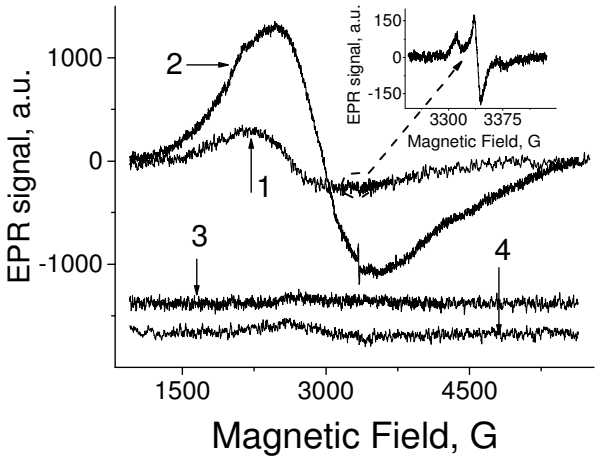

Fig. 2. EPR spectra of the initial unpurified chitosan sample X1 (*1*), initial (*2*) and purified (*3*) Celox samples; and solvent sample (succinic acid $C_4H_6O_4$) (*4*). Insert in Fig. 2: part of the EPR spectrum of sample X1, recorded with accumulation; this small signal belongs to nitroxyl radicals [4].

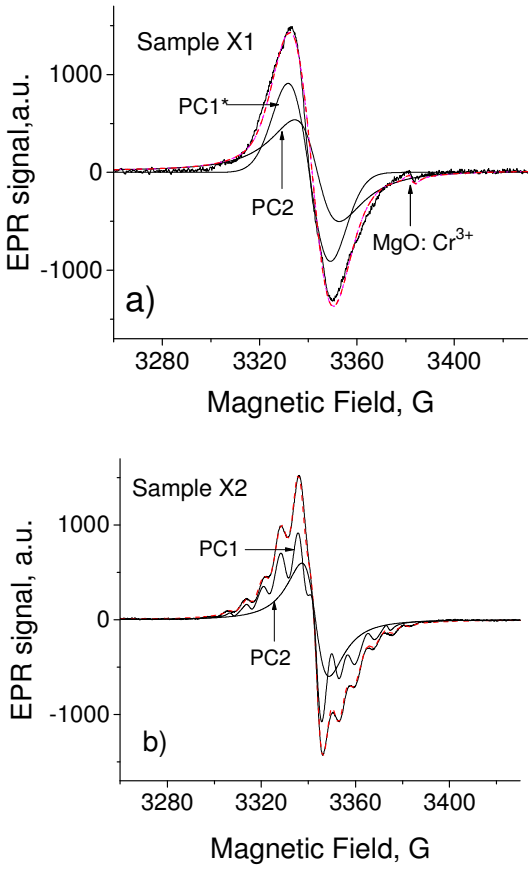

Fig. 3. EPR spectra for the samples X1 (a) and X2 (b) in some days after β-irradiation with the dose 25 kGy. Dashed lines are the result of fitting the theory with experiment. ν = 9373 MHz.

EPR transitions with nuclear spin $+I_z$ and 5 high-field lines for transitions with $-I_z$; as well as a wide central line that belongs to another spectrum. It should be emphasized that the observed SHFS spectrum is almost equidistant. It was found that if the dimensions of the crystallites in the sample X2 decrease to the submicron ones, SHFS is presented in the spectrum with poor resolution because of the greater width the separately components. It was found also that possible anisotropy of the *g*-factor and SHFS tensor *A* is not greater than the width of individual SHF components. Indeed, the EPR spectra recorded for a single crystallite of the sample X2 (~3×2×0.4 mm) at different orientations of the magnetic field relative to the plane of the sample (∥, ⊥, and at 45°) did not show any noticeable changes within the limits of measurement accuracy.

3.2. Analysis of the EPR spectra

First of all, let us address the question of the reason for the specific shape of the observed spectrum for powder sample X1 (Fig. 3a), which is characterized by a smaller amplitude of the peak high-field signal and a clearly observed bend near the center of the spectrum. There are two possible reasons for this feature. It could be either a single resonance line of the paramagnetic centers (PC) with an anisotropic *g*-tensor, or the spectrum of two resonance signals with slightly different isotropic *g*-factors.

To test the assumption 1, the signal was presented by the Lorentzian function with the resonance frequency $h\omega = \beta H \cdot g_{eff}$, depending on the angle θ between magnetic field *H* and the main axes of *g*-tensor: $g_{eff} = \left(g_{\parallel}^2 \cos^2\theta + g_{\perp}^2 \sin^2\theta\right)^{1/2}$ with $\left|g_{\parallel}^2 - g_{\perp}^2\right| \cdot \beta H$ comparable with the line width. The calculated absorption signal was averaged over the angle (θ), after that the result was differentiated for comparison with the experimental curve. The fitting to the experimental signal forced to abandon the first case, because the PC with an anisotropic *g*-tensor gives a high-field wing with a greater amplitude than the low-field one opposite to the experimental curve feature. Consequently, the spectra belong to a different paramagnetic centers (further PC1 and PC2) with the spin $S_1 = S_2 = 1/2$ and slightly different isotropic *g*-factors found to be equal to $g_{PC1} = 2.0048 \pm 3\cdot10^{-4}$, and $g_{PC2} = 2.0031 \pm 3\cdot10^{-4}$.

The spectrum for the sample X2 (Fig. 3b) was described by the theoretical function as a sum of eleven Lorentzian lines. Calculation of the theoretical spectrum and fitting to the experimental one was made in ORIGIN program, by using the least square method. The results of this fitting have been summarized in Table 1.

The analysis has shown that all the super-hyperfine lines (1 to 10 in Table 1) belong to the centers, the nature of which is below identified as being identical with the PC1 centers in the samples X1, but the SHF structure in which is not resolved due to greater amorphicity of the samples X1.

To understand what a free radical is with the SHFS structure found, let us suppose that electron spin interacts with some non-equivalent nuclei with the spin $I = 1/2$. The most probable candidates are hydrogen atoms in the structure shown in Fig. 1b. Hamiltonian of the system is as follows:

Table 1. Magnetic resonance field and EPR line width values for resonance transitions in the spectrum of Fig. 3b; ν = 9373 MHz.

Resonance line number	Experimental resonance field H_{res}, G	Line width ΔH_{pp}, G	Calculated H_{res} with constants from Table 2, G
1	3307.6	3.5	3307.6
2	3315.0	3.5	3315
3	3322.4	4.6	3322.7
4	3330.2	5.8	3330.2
5	3337.7	6.4	3337.3
6	3343.5	5.8	3344.0
7	3351.2	5.8	3351.4
8	3357.8	5.8	3359
9	3366.5	4.6	3366.5
10	3373.9	3.5	3373.9
11 (PC2)	3343.2	11.6	–

Table 2. Super-hyperfine constants for the paramagnetic centers PC1.

Number of nucleus	1	2	3	4
$\lvert A_{\parallel,j}\rvert$, G	28.6	15.5	14.8	7.4
$a_j \approx b_j$, G	9.5	5.2	4.9	2.5

$$H = g\beta H_z S_z + S_z \sum_1^4 A_{\parallel,j} I_{z,j} + 0.5 \cdot \sum_1^4 A_{\perp,j}\left(S_+ I_{-,j} + S_- I_{+,j}\right) \quad (1)$$

where $A_\parallel = a + 2b$, $A_\perp = a - b$ with the Fermi constant $a = \frac{8\pi}{3} \cdot g\beta g_n \beta_n \left|\psi(0)\right|^2$ and dipole-dipole constant $b = \frac{2}{3h} g\beta g_n \beta_n \left\langle r^{-3} \right\rangle$. The number of paramagnetic nuclei that interact with electron have to be larger than three, because three non-equivalent nuclei with $I = 1/2$ form only 2^3 states with the electron spin S_z. As soon as there are ten resonance transitions for PC1, the electron spin interacts with the minimum four non-equivalent nuclei (2^4 is enough to form ten transitions). The procedure is to find energies for 16 states of Hamiltonian (1), to calculate the resonance frequencies for 16 transitions and to compare with the experimental resonance fields from Table 1. The central point of the spectrum $H_{res,0}$ is found to be equal to 3340.75 G, which corresponds to g-factor $g_{(PC1)} = 2.0046$ ($\pm 3 \cdot 10^{-4}$). The total distance between the highest and lowest resonance transitions in Table 1 is equal to 66.3 G and in theory is $\Sigma_j A_{\parallel,j} - (1/2)\Sigma_j \left(A_{\perp,j}^2 / \omega_0\right)$. On the other hand, the latter high-field transition is distant from $H_{res,0}$ by $33.3\text{G} = -(1/2)\Sigma_j A_{\parallel,j} + (1/2)\Sigma_j \left(A_{\perp,j}^2 / \omega_0\right)$. These two equations give $\Sigma_j \left(A_{\perp,j}^2 / \omega_0\right) = 0.3G$ and consequently the 2-nd order contribution is negligible. In order to find 4 constants $A_{\parallel,j}$, it is enough to use 4 transitions from Table 1, after that to check the remaining resonance frequencies using the found constants. The accordance with the experimental resonance fields is satisfied. The calculated $A_{\parallel,j}$ values are given in Table 2; $\lvert A_{\perp,j}\rvert$ is less than the line width of SHFS component and has an order of the experimental error.

The obtained values of A_j and g-factor of the paramagnetic center PC1 indicate that the free radical is localized in the carbon position C5 of the chitosan structure. It has two nearest hydrogen atom and two distant hydrogen ones in the neighbor hydroxyl groups. The broader line 11 in Table 1 does not exhibit a visible SHF structure and by its characteristics completely coincides with the PC2 centers observed in the X1 samples: $g_{(PC2)} = 2.0031 \pm 3 \cdot 10^{-4}$; peak-to-peak line width $\Delta H_{pp} = 11.6$ G. The nature of the PC2 centers is most likely related to the carbon dangling bonds in the C1 position of the chitosan structure.

3.3. Microwave saturation experiments and spin relaxation of the paramagnetic centers

The relationship of centers PC1 and PC2 is justified by the saturation of the signals and the spin relaxation times, which are estimated by means of the signal continuous saturation method. Fig. 4a shows the measured EPR signals for the sample X2 at different microwave powers. Fig. 4b shows the saturation curves for the centers 1 and 2, which are in agreement with the theory of saturation of homogeneously broadened EPR signals [17]:

$$I\left(\left(\mathrm{P}/\mathrm{P}_{\max}\right)^{0.5}\right) = \text{const} \cdot \frac{\left(0.25\gamma^2 H_1^2 T_1 T_2\right)^{1/2}}{1 + 0.25\gamma^2 H_1^2 T_1 T_2}. \quad (2)$$

Here, $I = A_{pp} \cdot \left(\Delta H_{pp}\right)^2$, A_{pp} is the signal amplitude between extremes of the derivative of absorption, ΔH_{pp} – signal width between extremes, H_1 – amplitude of the microwave field, $\gamma = g\beta / h = 1.76 \cdot 10^7 \text{s}^{-1}$, β – Bohr magneton, T_1 and T_2 – spin-lattice and spin-spin relaxation times of PC. Adjustment (2) to the experimental curves allows finding the spin-relaxation times for these two PC. From Fig. 4b and formula (2), the value of the saturation factor was found

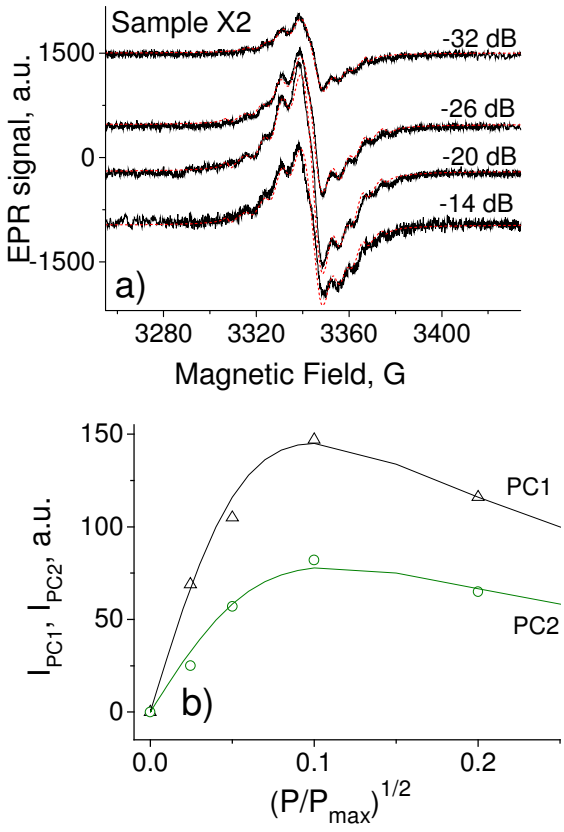

Fig. 4. a) EPR spectra for the sample X2 in some days after β-irradiation with 25 kGy at different levels of microwave power. Dashed lines are the result of fitting the theory with experiment. b) Signal saturation curves for the centers PC1 and PC2.

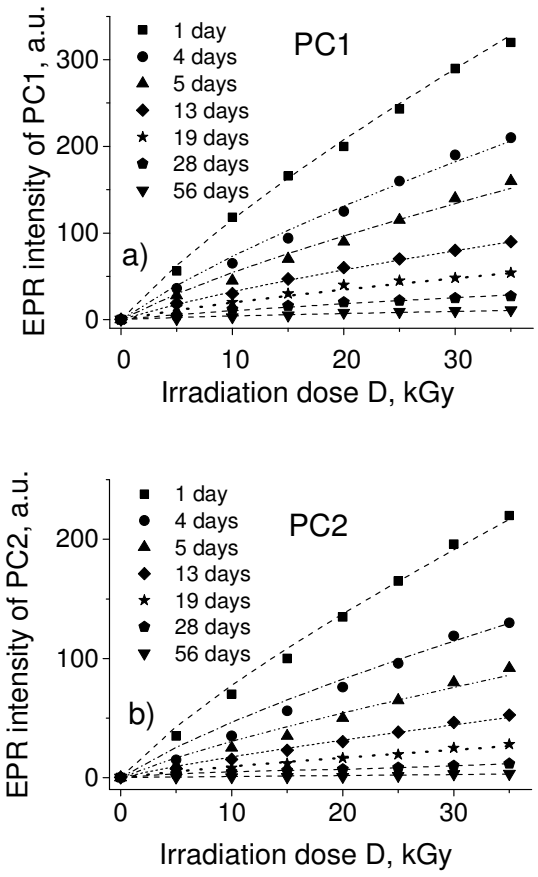

Fig. 5. Irradiation dose dependence of the integrated intensities for the paramagnetic centers PC1 (a) and PC2 (b) for different time intervals between the EPR recordings; symbols correspond to the experimental values, dashed lines – theoretical ones.

$S = 0.25\gamma^2 H_{1,\max}^2 T_1 T_2$, where $H_{1,\max} \approx 0.3$ G is the maximum value of the microwave field H_1, which are the characteristics of spectrometer. It was found $S_1 = 80$ for PC1 and $S_2 = 100$ for PC2. The spin-spin relaxation time $T_2 = 1.31 \cdot 10^{-7} / g / \Delta H_{pp}$, where ΔH_{pp} is given in Gauss unities. It is estimated for PC1 with the minimum line width of the lowest SHFS component 1 in Table 1 that $\Delta H_{pp} = 3.5$ G, and for PC2 with $\Delta H_{pp} = 11.6$ G. After that the spin-lattice relaxation time T_1 is obtained from S_1, S_2 values with $H_{1,\max} = 0.3$ G. The results are as follows:

$$\text{PC1}: T_2 = 1.9 \cdot 10^{-8}\,\text{s},\ T_1 = 0.6\,\text{ms};$$

$$\text{PC2}: T_2 = 0.56 \cdot 10^{-8}\,\text{s},\ T_1 = 2.6\,\text{ms}.$$

Paramagnetic spins, responsible for the broad signal PC2, have the shorter spin-spin relaxation time, but a longer spin-lattice relaxation time, since spin-lattice interaction in the disordered area is weakened as compared with that in the crystalline area. Measurements of the relaxation times of similar free radicals in γ-irradiated cellulose were carried out recently using the pulse saturation method [10]. The authors of this paper found T_2 by one order of value longer, but one order of value shorter T_1. The value of T_2 depends on the PC concentration, which was not determined in [10].

3.4. Irradiation dose dependence of paramagnetic response for samples X1

In this section, we consider the kinetics of the accumulation/decay processes of PC, depending on the dose of irradiation and subsequent storage of the samples in air.

The measurement procedure was as follows. The set of powdered chitosan samples X1 was irradiated using the beam of fast electrons with different doses. One day after irradiation, EPR signals were recorded for each sample with a certain radiation dose. Then the samples were stored for some time in air, after which recording the EPR spectra was repeated; this procedure was repeated many times. The results are given in Fig. 5. It is clearly seen that the concentration of free radicals gradually increases with increasing the radiation dose and decreases when the irradiated samples are stored in air. Separation of the EPR spectrum by two signals with the above *g*-factors was made for the EPR signals after each time interval. As a result, Fig. 5 demonstrates the dependence of the integrated intensity on both the radiation dose and time of sample storage in air. (The integrated intensity is proportional to the PC concentration.) As can be seen from Fig. 5, centers PC1 and PC2 show the similar dose dependences.

The experimental results shown in Fig. 5 by symbols are described by the calculated curves as the function of the irradiation dose *D*:

Table 3. Kinetic parameters that determine the dependence of N^+ on the exposure time of the samples in air after irradiation with the dose 35 kGy. The value $(N_0^+/N_0) = 0.17$ was found to be identical in all the cases.

Time, days		1	4	5	13	19	28	56
c_1, 10^3	PC1	0.11	0.08	0.05	0.03	0.016	0.007	0.002
c_2, 10^3	PC2	0.23	0.15	0.09	0.065	0.037	0.018	0.005
ξ_1, 10^{-3}	PC1	0.7	0.45	0.45	0.4	0.2	0.2	0.2
ξ_2, 10^{-3}	PC2	3	3	2.2	2	2	2	2
β_1, kGy^{-1}	PC1	0.16	0.14	0.15	0.14	0.14	0.13	0.14
β_2, kGy^{-1}	PC2	0.12	0.12	0.14	0.12	0.13	0.14	0.14

$$I_{1,2} = 0.17 + c_{1,2} \cdot (1 + \xi_{1,2} \cdot D) \cdot \left[(1 + \beta_{1,2} \cdot D)^{1/2} - 1 \right] . \quad (3)$$

Although the dose dependence is the same for signals 1 and 2, values I_1 and I_2 are different due to different parameters ξ, c, β given in Table 3.

Let us consider different processes that take part in creation of the paramagnetic radicals in the chitosan sample. Let N_0 be a total concentration of molecules able to become the free radical, both paramagnetic and non-paramagnetic; paramagnetic fraction of them N^+ is the concentration of free radicals; then $N_0 - N^+$ is the fraction of non-paramagnetic molecules, which becomes free radicals in the process of collision with irradiation particles; $\dot{n}$ is the concentration of electrons emerging after breaking the molecules and chains by collision with the irradiation particles; G is the generation rate of paramagnetic centers; W_t – rate of electron capture by traps created during structure destruction under the irradiation; R is the rate of the electron and paramagnetic center elimination in their collision. The kinetic equations for evolution of n and N^+ in the irradiation process are as follows:

$$\frac{\dot{n}}{N_0} = (W_{G,e} + W_{i,e}) - (W_{G,e} + W_{i,e} + W_t) \cdot \frac{n}{N_0} - W_R \cdot \frac{n}{N_0} \cdot \frac{N^+}{N_0},$$
$$\frac{\dot{N}^+}{N_0} = (W_G + W_i) - (W_G + W_i) \cdot \frac{N^+}{N_0} - W_R \cdot \frac{n}{N_0} \cdot \frac{N^+}{N_0} . \quad (4)$$

where W_G, $W_{G,e}$ are the probabilities of the birth of a free radical and free electron, which are in proportion to the radiation dose D: $W_G = \alpha D$, $W_{G,e} = \alpha_e D$, moreover $\alpha_e > \alpha$; $W_{i,e}$, W_i – probabilities of thermal ionization for atoms and molecules; W_t – probability of electron capture by traps, $W_R = R N_0$ – probability of recombination of electrons and free radicals. The stationary solution (at $t \to \infty$, $\dot{n} = 0$, $\dot{N}^+ = 0$) of the system (4) is accurately and reduces to a quadratic equation for N^+: $y^2 + cy = 0$, the solution of which can be represented in the following manner:

$$\frac{N^+}{N_0} = \frac{N_0^+}{N_0} + 0.5 \cdot c \cdot \left(\sqrt{(1 + \beta D)} - 1 \right),$$
$$\left(N_0^+ / N_0 \right) = N^+ (D = 0) / N_0 . \quad (5)$$

Here,

$$c = c_0 (1 + \xi D), \; c_0 = (W_{i,e} / W_i) + (W_t + W_{i,e}) / W_R ,$$
$$\xi = \alpha_e \cdot W_i / (W_{i,e} \cdot W_R + W_i \cdot W_t) << 1, \; \beta = \alpha_e / (W_{i,e} + W_t). \quad (5a)$$

Comparison of (5) with (3) and Table 3 leads to the conclusion that the concentration of PC is determined by the rate of generation and by the ratio of capture rates on traps and paramagnetic centers, *i.e.*, c_0 is the greatest value and the most variable with the time duration after irradiation. In the expression for c_0 (5a), there is one quantity only, which is the largest and it varies appreciably as the sample return to equilibrium, it is the rate of the electron capture by the traps; thus $c_0 \approx W_t / W_R$.

All above processes are fast; however, after irradiation there are also seen slow processes, which in the measurement (see Fig. 5) can be seen as a steady decrease in the value N^+ at any dose, after several days of waiting between measurements. Especially brightly, this property appears at the maximum irradiation dose.

3.5. Decay of the paramagnetic centers concentration during storage of irradiated samples in air

Fig. 6 shows the dependences of the radical concentration on the waiting time between successive measurements of the EPR signal. These dependences is described by the two-exponential function with the times τ_1 and τ_2 exponential decay and shown in Fig. 6 by dashed lines. One can see that the values of intensities are varied by an order for fifty days. Table 3 shows that the kinetic characteristic also changed with time an order of magnitude which is a property of W_t. Thus, the main feature of the material is the release of electrons from traps that are the result of the interatomic bond breaking under irradiation and atom shifts from the sites. These traps are not paramagnetic; they are extended formations, and disappear with time, which is necessary for the recovering of the molecular system in structural relaxation process.

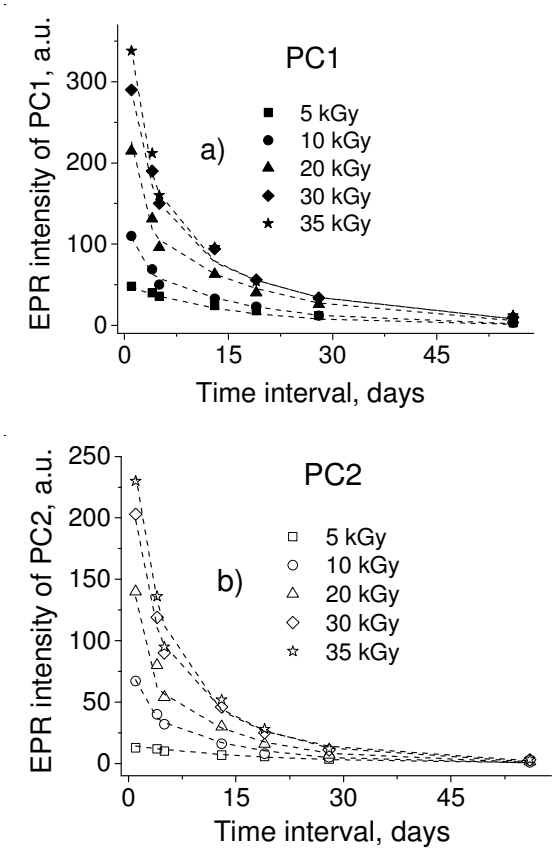

Fig. 6. Decay of PC1 (a) and PC2 (b) concentrations with time after irradiation of the samples X1 with different doses; symbols – experiment, dashed lines – theory.

Table 4. Structure recovery time and the weight factors of the respective exponential functions.

Dose, kGy	PC1				PC2			
	Weight of the 1st exponent	$\tau_{0,1,1}$ days	Weight of the 2nd exponent	$\tau_{0,1,2}$ days	Weight of the 1st exponent	$\tau_{0,2,1}$ days	Weight of the 2nd exponent	$\tau_{0,2,2}$ days
5	0.17	18	0.83	0.5	0.4	15	0.6	1
10	0.45	12	0.55	1	0.47	15	0.53	1
20	0.41	12	0.59	1	0.35	17	0.65	1
30	0.48	12	0.52	2	0.39	19	0.61	2.8
35	0.36	14	0.64	3	0.36	19	0.64	3

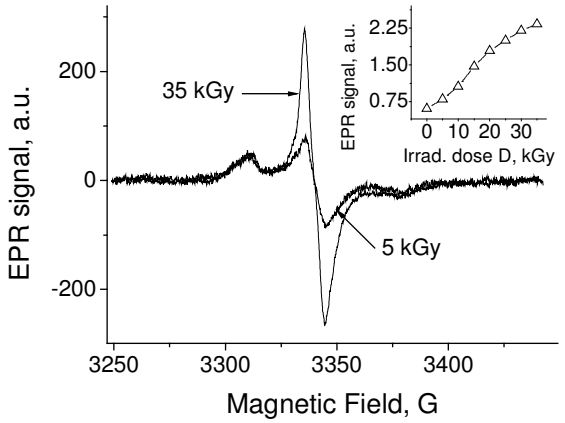

Fig. 7. EPR spectra of the samples X1 2 years after irradiation with the doses 5 and 35 kGy (recorded with accumulation). The central line is the total contribution of nitroxyl radicals and PCl centers; the side components are due to nitroxyl radicals only [4]. Insert in Fig. 7: the intensity of the central line of spectrum as a function of the irradiation dose.

The dashed lines, which describe the experimental data in Fig. 6, are calculated according to the functions:

$$I_i(t) = I_{0,i} + A_{i1} \cdot \exp\left(-t/\tau_{0,i,l}\right) + A_{i2} \cdot \exp\left(-t/\tau_{0,i,2}\right) , \quad (6)$$

where A_{i1}, A_{i2} are weight factors for the exponential functions. All the parameters in Eq. (6) are given in Table 4. Note that the contribution of the fast exponential function is 60% and is essentially independent of the dose. The same dependence shows that W_t, obviously at the expense of reducing the number of traps due to the ionization and their decay in the process of diffusion of atoms.

Electrons of irradiation are captured by the traps after irradiation turning off. In the process of recovering, the number of traps is reduced by the amount of $\delta N(t) = N_{t0} \exp\left(-W_D t\right)$, where W_D is the atom diffusion rate, and n is increased as the $n = n_0 + \delta n$ with $\delta n = \delta N(t)$. Therefore, in this case:

$$N^+/N_0 = \left(W_G/R_{n_0}\right) \cdot \left(1 - \left(N_t/n_0\right)\right) \cdot \exp\left(-W_D t\right). \quad (7)$$

Irradiation of the material leads to a large number of traps with low potential barrier, which disappear for one or two days. Traps with higher barriers are able to keep electrons for 15…19 days. This property is a proper characteristic of the material and does not depend on the radiation dose.

It is important to note that the paramagnetic defects in the crystalline samples X2 are much more stable, and their concentration decreases for one year by about 5 times, while those in the samples X1 decrease by one order of value for 2 to 3 months. It is related with higher extent of the crystallinity in the samples X2.

Finally, with regard to the behavior of nitroxyl centers (Fig. 2, inset), one can say their EPR intensity almost does not change upon irradiation with these small doses that were used in our experiments. However, 2 years after irradiation, the PC2 centers completely disintegrate, while the more stable nitroxyl radicals and the residual spectrum of PC1 are still recorded, albeit in a small concentration. Shown in Fig. 7 is the EPR spectrum in the chitosan sample X1 2 years after irradiation with the dose 35 kGy. It can be seen that only nitroxyl radicals and residual signal of PC1 centers (main contribution to the central line of spectrum) are recorded. The insert to Fig. 7 shows that there is an approximately linear relationship between the dose of chitosan samples irradiation and the intensity of the central line 2 years after irradiation.

4. Conclusion

The observed EPR spectra were described by the sum of two EPR signals PC1 and PC2 with the spin $S = 1/2$, Lorentz line shape, different g-factors and different line widths. For PC1: $g_{PC1} = 2.0047 \pm 4 \cdot 10^{-4}$, $\Delta H_{pp,1} = 3.5…6.4$ G and 9 G for separately SHF components in the samples X2 and the envelope of the spectrum in samples X1, accordingly. For PC2: $g_{PC2} = 2.0031 \pm 3 \cdot 10^{-4}$, $\Delta H_{pp,2} \cong 12$ G. Based on the first time observed well-resolved SHF structure of the spectrum in the "crystalline" samples, it has been ascertained that the radicals PC1 are characterized by the electron state located at the site C5 and has the SHF interaction with four hydrogen atoms from the molecule CH_2OH and two neighbor hydroxyl groups with $A_{\|,j} = 28.6$, 15.5, 14.8, 7.4 G. The value of g-factor is found to be 2.0047, which is close to the obtained one in [10]. The 2-nd order

correction $|A_{\perp,j}|^2$ has the small values and gives a contribution only to the line width of SHFS components. By this reason, the width of these lines increases from the distant components to the central ones, which is observed in the experimental spectrum of X2 samples.

The second wider signal PC2 belongs to dangling bonds of carbon localized most probably in C1 position of the chitosan structure and does not show the super-hyperfine structure. It has been found the functional dependence of EPR signals on the irradiation dose. The achieved concentration of radicals decreases with time after irradiation along the two-exponential law with the characteristic times $\tau_{0,1,1}$ = 12…18 days, $\tau_{0,1,2}$ = 15…19 days, $\tau_{0,2,1}$ = 0.5…3 days, $\tau_{0,2,2}(2)$ = 1…3 days, being dependent on the irradiation dose. The long time decay contributes only about 40% to the intensity decrease. Higher stability of radicals in samples with a more crystalline structure has been observed.

Thus, irradiation of chitosan with fast electrons in sterilization doses leads to the appearance of a significant concentration of paramagnetic defects that disintegrates gradually, but not fully, at prolonged storage of the samples in air.

Acknowledgement

The authors of the paper are grateful for support by National Academy of Science of Ukraine (Project № 26/17-H).

References

1. Baskar D., Sampath Kumar T. S. Effect of deacetylation time on the preparation, properties and swelling behavior of chitosan films. *Carbohydrate Polymers*. 2009. **78**. P. 767–772.
2. Chmielewski A.G., Migdal W., Swietoslawski J., Jakubaszek U., Tarnowski T. Chemical-radiation degradation of natural oligoamino-polysaccharides for agricultural application. *Radiation Phys. and Chem*. 2007. **76**. P. 1840–1842.
3. Dumitrin S., Popa M.I., Cringu A., Stratone A. Bioactive polymers 61. Synthesis and characterization of some retard antibiotics. *Colloid. Polym. Sci*. 1989. **267**. P. 595–599.
4. Gryczka D., Dondi A.G., Chmielewski W., Migdal A., Buttafava A., Faucitano A. The mechanism of chitosan degradation by gamma and e-beam irradiation. *Radiation Phys. and Chem*. 2009. **78**. P. 543–548.
5. Gaill F., Shillito B., Lechaire J. P., Chanzy H., Goffinet G. The chitin secreting system from deep sea hydrothermal vent worms. *Biol Cell*. 1997. **76**. P. 201–204.
6. Jae-Young J., Se-Kwon K. Antioxidant activity of novel chitin derivative. Bioorganic and *Medicinal Chem. Lett.* 2006. **16**. P. 1884–1887.
7. Kumirska J., Czerwicka M., Kaczynski Z., Bychowska A., Brzozowski K., Thöming J., Stepnowski P. Application of spectroscopic methods for structural analysis of chitin and chitosan. *Mar. Drugs*. 2010. **8**. P. 1567–1636.
8. Kumirska J., Weinhold M.X., Thöming J., Stepnowski P. Biomedical activity of chitin/chitosan based materials – influence of physicochemical properties apart from molecular weight and degree of N-acetylation. *Polymers*. 2011. **3**, No 4. P. 1875–1901.
9. Kashappa G.D., Hyum J.P. Study of gamma-irradiation effects on chitosan microparticles. *Drug Delivery*. 2006. **13**. P. 39–50.
10. Kameya H., Kikuchi M., Hara H., Furuta M., Todoriki S., Kobayashi Y., Ukai M., Shimoyama Yu. Relaxation behaviors of free radicals from γ-irradiated black pepper using pulsed EPR spectroscopy. *Appl. Magn. Reson*. 2012. **42**. P. 153–159.
11. Marguerite R. Chitin and chitosan: Properties and applications. *Prog. Polym. Sci*. 2006. **31**. P. 603–632.
12. Mironenko A.Yu., Sergeev A.A., Nazirov A.E., Modin E.B., Voznesenskiy S.S., Bratskaya S.Yu. H_2S optical waveguide gas sensors based on chitosan/Au and chitosan/Ag nanocomposites. *Sensors and Actuators B*. 2016. **225**. P. 348–353.
13. Minke R., Blackwell J. The structure of α-chitin. *J. Mol. Biol.* 1978. **120**. P. 167–181.
14. Ngah W.S.W., Ghani S.A., Kamari A. Adsorption behaviour of Fe(II) and Fe(III) ions in aqueous solution on chitosan and cross-linked chitosan beads. *Bioresour. Technol*. 2005. **96**. P. 443–450.
15. Peniche C.C., Alwarez L.W., Arguelles M.W. The adsorption of mercuric ions by chitosan. *J. Appl. Polym. Sci.* 1987. **46**. P. 1147–1150.
16. Pasanphan W., Buettner G.R., Chirachanchai S. Chitosan gallate as a novel potential polysaccharide antioxidant: an EPR study. *Carbohydrate Res.* 2010. **345**. P. 132–140.
17. Poole C.P.Jr. *Electron Spin Resonance: A Comprehensive Treatise on Experimental Techniques*, Second ed. Dover, Delaware 2010.
18. Potara M., Baia M., Farcau C., Astilean S. Chitosan-coated anisotropic silver nanoparticles as a SERS substrate for single-molecule detection. *Nanotechnology*. 2012. **23**, No 10; doi:10.1088/0957-4484/23/5/055501.
19. Richardson S.C., Kolbe H.V., Duncan R. Potential of low molecular mass chitosan as a DNA delivery system: Biocompatibility, body distribution and ability to complex and protect DNA. *Int. J. Pharm.* 1999. **178**. P. 231–243.
20. Roberts G.A.F. The road is long.... Advances in chitin science, vol. X. *Proc. 8th intern. conf. of the European chitin society,* 8–11 September 2007, Antalya, Turkey. Senel S., Varum K.M., Sumnu M.M., Hincal A.A., Eds. P. 3–9.
21. Riccardo A.A.M., Tanfani F., Scarpini G., Muzzarelli M.G. ESR Characterization of chitins and chitosans. *Biochem. and Biophys. Res. Com*. 1979. **89**. P. 706–712.

22. Szymanska E., Winnicka K. Stability of chitosan – a challenge for pharmaceutical and biomedical applications. *Marine Drugs*. 2015. **13**. P. 1819.
23. Sudarshan N.R., Hoover D.G., Knorr D. Antibacterial action of chitosan. *Food Biotechnol.* 1992. **6**. P. 257–272.
24. Wenjun L.I., Xuan J., Peihua X., Shiming C. H. Inhibitory effects of chitosan on superoxide anion radicals and lipid free radicals. *Chin. Scince Bull*. 2002. **47**. P. 887–889.
25. Yamamoto H., Amaika M. Biodegradation of cross-linked chitosan gels by a microorganism. *Macromolecules*. 1997. **30**. P. 3936–3937.

Authors and CV

Andriy Andriyovich Konchits.
Dr. A.A. Konchits is a leading scientist of the Department Optics and Spectroscopy at the V.E. Lashkaryov Institute of Semiconductor Physics NAS of Ukraine.
His main research interests include the nanostructured materials and composites. Also, he has been working on porous materials (porous coal), their structure, and electrical properties.
E-mail: konchits@ukr.net

Bela Dmytrivna Shanina
Dr. Shanina B.D. is a professor and a leading researcher of the Department Optics and Spectroscopy at the V.E. Lashkaryov Institute of Semiconductor Physics NAS of Ukraine. Her research areas are electronic properties of nanostructured materials.
E-mail: shanina_bela@rambler.ru

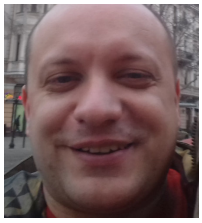

Igor Bogdanovich Yanchuk
Igor Bogdanovich Yanchuk is a PhD of the Department Biotechnology at the Farmak. His main research interests include the correlation of structural features of carbon materials with their optical and mechanical properties.
E-mail: i.b.yanchuk@gmail.com

Serhii Volodymyrovich Krasnovyd.
Mr. Krasnovyd S.V. is junior researcher of the Department Optics and Spectroscopy at the V.E. Lashkaryov Institute of Semiconductor Physics NAS of Ukraine. His main research interests are the nanostructured materials, their electronic properties.
E-mail: sergkrasnovyd@gmail.com